Regularization in Deformable Registration of Biomedical Images Based on Divergence and Curl Operators

S. Riyahi-Alam[1]; M. Peroni[2]; G. Baroni[3,4]; M. Riboldi[3,4]

[1]Department of Mechanical and Aerospace, Biomedical Engineering, Politecnico di Torino, Torino, Italy;
[2]Paul Scherrer Institut, Zentrum für Protonentherapie, WMSA/C15, Villigen PSI, Switzerland;
[3]Dipartimento di Elettronica, Informazione e Bioingegneria, Politecnico di Milano, Milano, Italy;
[3]Bioengineering Unit, Centro Nazionale di Adroterapia Oncologica, Pavia, Italy

Keywords

Deformable image registration, divergence and curl, multi-resolution registration, landmark based evaluation

Summary

Background: Similarity measures in medical images do not uniquely determine the correspondence between two voxels in deformable image registration. Uncertainties in the final computed deformation exist, questioning the actual physiological consistency of the deformation between the two images.

Objectives: We developed a deformable image registration method that regularizes the deformation field in order to model a deformation with physiological properties, relying on vector calculus based operators as a regularization function.

Method: We implemented a 3D multi-resolution parametric deformable image registration, containing divergence and curl of the deformation field as regularization terms. Exploiting a BSpline model, we fit the transformation to optimize histogram-based mutual information similarity measure. In order to account for compression/expansion, we extract sink/source/circulation components as irregularities in the warped image and compensate them. The registration performance was evaluated using Jacobian determinant of the deformation field, inverse-consistency, landmark errors and residual image difference along with displacement field errors. Finally, we compare our results to a robust combination of second derivative regularization, as well as to non-regularized methods.

Results: The implementation was tested on synthetic phantoms and clinical data, leading to increased image similarity and reduced inverse-consistency errors. The statistical analysis on clinical cases showed that regularized methods are able to achieve better image similarity than non regularized methods. Also, divergence/curl regularization improves anatomical landmark errors compared to second derivative regularization.

Conclusion: The implemented divergence/curl regularization was successfully tested, leading to promising results in comparison with competitive regularization methods. Future work is required to establish parameter tuning and reduce the computational cost.

Correspondence to:
Sadegh Riyahi-Alam
Department of Mechanical and
Aerospace Biomedical Engineering
Politecnico di Torino
Corso Duca degli Abruzzi n. 24
10129 Torino
Italy
E-mail: sadegh.riyahi@polito.it

Methods Inf Med 2014; 53: 21–28
doi: 10.3414/ME12-01-0109
received: December 1, 2012 accepted:
July 21, 2013 prepublished:
November 5, 2013

1. Introduction

Image Registration is the process of defin-ing the transformation between two images so that the coordinates in one image (mov-ing) correspond to those in the other (fixed). Deformable Image Registration (DIR) includes a model of deformation in the transformation, and it is widely used for the analysis of medical images. In a radiation therapy clinical workflow, DIR provides a framework to perform contour propagation, tumor tracking at planning or treatment stage, as well as deformation quantification at follow-up [1–7] and treat-ment volume margins customization to po-tentially reduce dose to healthy tissues. [8]

The chosen similarity model between fixed and warped moving images should ensure the smoothness of final deformation field (DF) [1– 8], as topology er-rors in the DF imply that the transfor -mation is not consistent with physiological/anatomical deformation. In order to com-pensate such irregularities, authors gen-erally introduce a regularization term in the cost function [9, 10] or post-process the calculated DF [11]. Consistent image registration is also often applied to allow simultaneous registration of images in two directions (direct and inverse).

Sorzano et al. [12] used divergence and curl operators of the DF as the regulariza -tion function in 2D elastic registration for molecular-biological images along with Sum of Squared Difference (SSD) data term. Divergence (div) operator of a DF is used as a vector spline regularization func-tion to compensate the dilation/narrowing density of the field, and helps detecting sinks/sources emerged during the registration process. Likewise, the curl operator

reduces the rotation in a field and quantifies changes in orientation and vorticity in a DF. The framework was further extended to encompass an inverse consistency term in the cost function [13].

In this paper, we focus on compensating irregularities detected in the DF by exploiting divergence and curl operators as a regularization function. We extended the previous method by Sorzano [12] by implementing a multi-resolution 3-dimensional parametric deformable registration, characterized by cubic BSpline transformation, using a combination of Mutual Information (MI) [14] as similarity metric and div-curl regularization term, simultaneously optimized using ITK libraries [15]. Regularization based on divergence and curl has been applied so far on biological binary 2D images, not appropriate for histogram-based similarity metric, and for accurate quantitative evaluation [12]. Our method is modeled to mostly focus on anatomical areas where undesired compression/expansion irregularities in the vector field may significantly alter the smoothness of physiological motion and compromise clinical use. At each stage, optimally weighted div and curl parameters are provided to balance each term contribution in the cost function. The implemented registration framework is applicable to multi-modal registration, as no constraints exist on the absolute intensity values in the images to be registered.

To prove the performance of our application, we tested the proposed approach on a 3D CT of a head and neck phantom and 4D lung CT clinical images. We exploited landmark error evaluation as the most reliable metric in registration assessment [16], along with MI, jacobian determinant, inverse consistency and displacement field errors to demonstrate that the final DF reduced misalignment errors, leading to an overall registration improvement. Eventually, we compared our method with a publicly available regularization method [17], as well as with non-regularized only-MI registration.

2. Methods and Implementation

2.1 Cost Function Definition

Our multi-resolution registration scheme includes rigid and affine linear registration followed by a coarse and a fine BSpline nonlinear deformation stages. Coarse grid registration is performed by defining a 12 ξ 12 ξ 12 BSpline grid of control points, which is increased to 30 ξ 30 ξ 30 for the fine stage, thus decreasing the physical grid spacing accordingly.

In each non rigid stage, we optimize the following cost function:

$$C(x,y,z) = E_{sim} + w_d E_{div} + w_c E_{curl} \quad (1)$$

where E_{sim} is the similarity between fixed and moving image (MI), and E_{div} and E_{curl} rep-resent div and curl of the current DF as the regularization term, weighted by w_d and w_c (see Section 2.2). E_{sim} is increased during the optimization process performed by gradient descent, whereas the regularization term is decreased until violating one of the stopping criteria (gradient magnitude tolerance and minimum step length are set to 0.0001 and maximum number of iterations at 500).

The implementation of our cost func-tion requires the definition of a new strat-egy to combine a term directly dependent on image intensities (E_{sim}) and a weighted sum of derivatives of the current DF at each voxel (E_{div} and E_{curl}).

2.2 Embedding Divergence and Curl into the Cost Function

In Equation 1, we define

$$E_{div} = \sum_{i}^{N}\sum_{j}^{M} Div\,T_{ij}^2 \quad (2)$$

$$E_{curl} = \sum_{i}^{N}\sum_{j}^{M} Curl\,T_{ij}^2 \quad (3)$$

where T is the DF characterized by the BSpline control point coefficients, i is the current voxel ($i = 1 : N$) and j the spatial component for each voxel ($j = 1 : M$).

Divergence and curl are defined as can be seen in Equation 4 and Figure 1.

$$Div\,T(x,y,z) = \partial T_x/\partial x + \partial T_y/\partial y + \partial T_z/\partial z \quad (4)$$

Divergence and curl of a vector field quantify the total amount of deformation that is applied. Divergence operator is a scalar function (Eq. 4) and only specifies the changes in scale at each component of the DF, whereas the curl operator is a vector function and represents the circulation density of the DF. The magnitude and direction of $Curl\,T$ (Eq. 5) represent, respectively, the speed of rotation and the trajectory of the deformation.

Theoretically div/curl operators should be computed at each voxel, but in order to be able to combine these with an image similarity term, we propose to evaluate their L_2 norm on the regions correlated to BSpline grid control points, separately for each component direction.

Therefore, in order to compute the divergence term at each iteration of the optimizer, we proceed as follows:

1. Split the components of DF at the previous iteration.
2. Compute the necessary directional derivatives $\partial T_x/\partial x$, $\partial T_y/\partial y$ and $\partial T_z/\partial z$ by using the central finite difference scheme.
3. Combine the vector gradient components together to construct $\partial T_x/\partial x + \partial T_y/\partial y + \partial T_z/\partial z$
4. Calculate divergence as the L_2 norm of the gradient magnitude of each vector component.
5. Apply user-defined weight w_d to balance the divergence contribution in the final cost function value.

An analogous workflow is followed for the calculation of the curl term.

The final cost function equation becomes therefore as can be seen in Figure 2, which is the multi-modal extension

$$Curl\,T(x,y,z) = \left(\partial T_z/\partial y - \partial T_y/\partial z\right)\vec{i} + \left(\partial T_x/\partial z - \partial T_z/\partial x\right)\vec{j} + \left(\partial T_y/\partial x - \partial T_x/\partial y\right)\vec{k}$$

Figure 1 Definition of curl operator

$$C(x,y,z) = -\left[H(I_f) + H(I_m) - H(I_f, I_m)\right] + \sum w_d Div T(x,y,z)^2 + \sum w_c Curl T(x,y,z)^2$$

Figure 2 Final cost function equation

of the 2D volume described in [12]. $H(I_f)$, $H(I_m)$ denote entropies for fixed and moving images and the minus sign before MI accounts for the fact that the similarity metric must be maximized, as opposed to the regularization term.

2.3 Image Dataset

We first tested our approach on an image of a RANDO® (The phantom laboratory, Salem, NY) dosimetric phantom acquired on a clinical CT scanner (GE Medical System Light Speed, Fairfield, CT), using supine setup and clinical acquisition protocols. The volume acquired features 512 ξ 512 ξ 123 voxels and [0.94, 0.94, 3] mm el-ement spacing, which we subsample by a factor of 2. We applied three synthetic non-rigid deformations, specifically designed for head-neck district, to the images. This was achieved by superimposing three dif-ferent Gaussians, as described in [18]. The obtained DF is then used to evaluate the registration error.

Our method is also applied to five clinical datasets obtained from (www.dir-lab.com) belonging to different patients. Since the datasets are provided with pathology approved landmarks on extreme phase im-ages, we used them as a robust benchmark to evaluate our application. Image charac-teristics of the clinical studies are summarized in Table 1. ClinicCase1 represents minimum deformation, whereas ClinicCases4 and 5 stand for the largest deformation, as demonstrated by the average landmark displacement column. Subsampling resolution applied for each volume is also presented.

2.4 Evaluation Methods

Evaluation of non-rigid image registration algorithm is a hard task, since point-wise correspondence between two registered images is typically not known [19]. We used a combination of metrics to better describe the different aspects of deformable registration in both datasets, as proposed also by [20].

In order to assess the smoothness of DF in the synthetic dataset, Root Mean Square (RMS) of the difference between the synthetic (ground-truth) and the obtained DF is calculated. Normalized Mutual Information (NMI) between the fixed and warped images is computed for both datasets, as a residual image difference.

For clinical cases, where we are not supplied with the synthetic DF, we verified the average 3D displacement between landmarks individuated on each fixed and moving image of the clinical dataset, which is considered the most robust evaluation metric [16].

We further verified the inverse consistency of our method on the clinical dataset, along with the jacobian determinant of the transformation for both datasets, in order to ensure the bijective mapping (non-singularity/invertibility) and indicate irregularities in the transformation.

2.5 Plastimatch regularization method

We compared our method with Plastimatch [17] BSpline registration application, featuring MI as similarity metric and a second derivative of the DF as a robust regularization term [21]. The regularization used here is the squared of the DF t = (t_x, t_y, t_z) second derivatives, which is computed as shown in Figure 3.

Therefore, we applied the registration on the same clinical dataset using the same registration parameters i.e. Bspline grid points, subsampling resolution and number of iterations applied on our registration to compare the warping performance according to all the evaluation metrics.

3. Results

3.1 Synthetic Phantom

For this dataset, we obtained the smoothest DF and the best similarities of fixed and warped images using w_d and w_c both set to 0.1 for coarse stage and 0 for w_d and w_c in the fine stage respectively.

The RMS displacement when optimum weights are used is 4.69 mm, whereas MI-only with no regularization reaches 5.09 mm residual error.

Minimum jacobian of our SyntheticCase is as high as 0.79 (Table 2), suggesting that refinement of irregularities during the registration process done by our method resulted in a smoother DF comparing to 0.73 for the original ground-truth synthetic DF. In Table 2 final registration results of our DivCurl method, compared with non regularized MI-only registration for synthetic cases and Plastimatch (PLM) method for clinical cases are reported.

$$E_{reg} = \int E_{reg,x} + E_{reg,y} + E_{reg,z}$$

where

$$E_{reg,x} = \left(\frac{\partial t_x^2}{\partial x^2}\right)^2 + \left(\frac{\partial t_x^2}{\partial y^2}\right)^2 + \left(\frac{\partial t_x^2}{\partial z^2}\right)^2 + \left(\frac{\partial t_x^2}{\partial x \partial y}\right)^2 + \left(\frac{\partial t_x^2}{\partial x \partial z}\right)^2 + \left(\frac{\partial t_x^2}{\partial y \partial z}\right)^2$$

Figure 3 Plastimatch regularization term

Table 1 Specification of the clinical cases, selected to test our registration framework

Cases	Image dimension	Voxel dimension (mm)	Avg landmark displacement (mm)	Subsampling res.
ClinicCase1	256 x 256 x 94	0.97 x 0.97 x 2.5	4.01	[1 1 1]
ClinicCase2	256 x 256 x 99	1.13 x 1.13 x 2.5	9.42	[1 1 1]
ClinicCase3	256 x 256 x 106	1.10 x 1.10 x 2.5	7.10	[1 1 1]
ClinicCase4	512 x 512 x 136	0.97 x 0.97 x 2.5	11.59	[2 2 1]
ClinicCase5	512 x 512 x 128	0.97 x 0.97 x 2.5	15.16	[2 2 1]

3.2 Real Patient Clinical Cases

Quantitatively, DivCurl and PLM did not show large appreciable differences in terms of image similarity. For instance in ClinicCase1, PLM resulted in NMI image similarity values as high as 0.60 (of 1), whereas 0.64 NMI was measured for DivCurl. Residual errors between the fixed and warped landmarks were statistically compared relying on the non parametric Friedman test (at 99% confidence). Residual errors were significantly different in all clinical cases. The post-hoc comparison highlighted that PLM had significantly larger errors in 4 out of 5 cases, if compared to the DivCurl and MI methods (group H in the last column of Table 2). No appreciable difference was obtained in inverse consistency error for both methods, which measured 2.87 mm for DivCurl and 2.9 mm for PLM. MI-only non-regularized registration method resulted in a less smooth DF, as testified by a higher inverse consistency error (>3 mm) as well as NMI which is small as 0.58. For ClinicCase5, regularization weights larger than 0.1 produced a negative minimum jacobian value, i.e. a non-smooth DF: similar results were achieved by all other methods.

For qualitative evaluation, in Figure 4 we present the final DF overlaid on a slice belonging to both synthetic and clinical cases. Figures in first row of panel (a) show fixed and moving images belonging to synthetic case respectively, and images in bottom row show warped images belonging to Only-MI and DivCurl method with optimum weights. Bold white arrows indicate the most discriminative areas in each image, corresponding to large irregularities that were compensated during the registration with DivCurl. In panel (b), first row represents fixed and moving images for ClinicCase1, whereas the bottom row presents deformed moving images for Div-

Table 2 A Quantitative registration results belonging to both synthetic and clinical cases are presented along with the assigned weights for our divcurl method, plastimatch (PLM) and only-mi method. Here the only best case resulting from tuning the weights of div/curl are presented. For the synthetic cases we are not provided by the landmark features on the images, likewise the clinical cases are not supplied with the synthetic DF to calculate the avg 3D RMS displacement. Moreover, the inverse consistency is only evaluated on the clinical cases. Group (H) in the landmark error evaluation denotes the methods with significantly higher residual errors measured on the landmarks. (W_{dc}, W_{cc} = div/curl weight in coarse stage, W_{df}, W_{cf} = div/curl weight in fine stage, (H) significantly different)

Cases/metrics	[W_{dc}, W_{cc}, W_{df}, W_{cf}]	Iterations [Coarse, Fine]	NMI (of 1)	RMS disp. field (mm)	Min. Jacobian	Inverse cons. (mm)	Landmark error fixed, moving (mm)	Landmark error fixed, warped (mm)
SyntheticCase-DivCurl	[0.1, 0.10, 0]	[217,32]	0.68	4.69	0.79	–	–	–
SyntheticCase-MI	–	[145,16]	0.65	5.09	0.78	–	–	–
ClinicCase1-DivCurl	[0.5, 0.50.5, 0.5]	[401,78]	0.64	-	0.44	2.87	3.89	1.42
ClinicCase1-PLM	–		0.60	-	0.69	2.90	3.89	1.68 (*H*)
ClinicCase1-MI	–	[291,41]	0.58	-	0.33	3.22	3.89	1.36
ClinicCase2-DivCurl	[1, 10, 0]	[500,305]	0.53	-	0.11	0.94	9.83	2.80
ClinicCase2-PLM	–		0.50	-	0.53	0.95	9.83	4.07 (*H*)
ClinicCase2-MI	–	[320,186]	0.50	-	0.05	1.27	9.83	2.97
ClinicCase3-DivCurl	[0.1, 0.10, 0]	[500,500]	0.53	-	0.01	1.8	7.48	3.57
ClinicCase3-PLM	–		0.48	-	0.37	2.2	7.48	4.14 (*H*)
ClinicCase3-MI	–	[500,263]	0.48	-	–0.07	2.97	7.48	3.52
ClinicCase4-DivCurl	[0.1, 0.10, 0]	[500,496]	0.53	-	0.24	2.60	11.03	4.40 (*H*)
ClinicCase4-PLM	–		0.50	-	0.70	2.64	11.03	3.69
ClinicCase4-MI	–	[500,234]	0.50	-	0.30	3.78	11.03	4.38 (*H*)
ClinicCase5-DivCurl	[0.1, 0.10, 0]	[500,500]	0.49	-	–0.22	3.56	14.99	4.47
ClinicCase5-PLM	–		0.48	-	–0.01	4.09	14.99	5.53 (*H*)
ClinicCase5-MI	–	[500,346]	0.47	-	–0.20	4.34	14.99	5.00

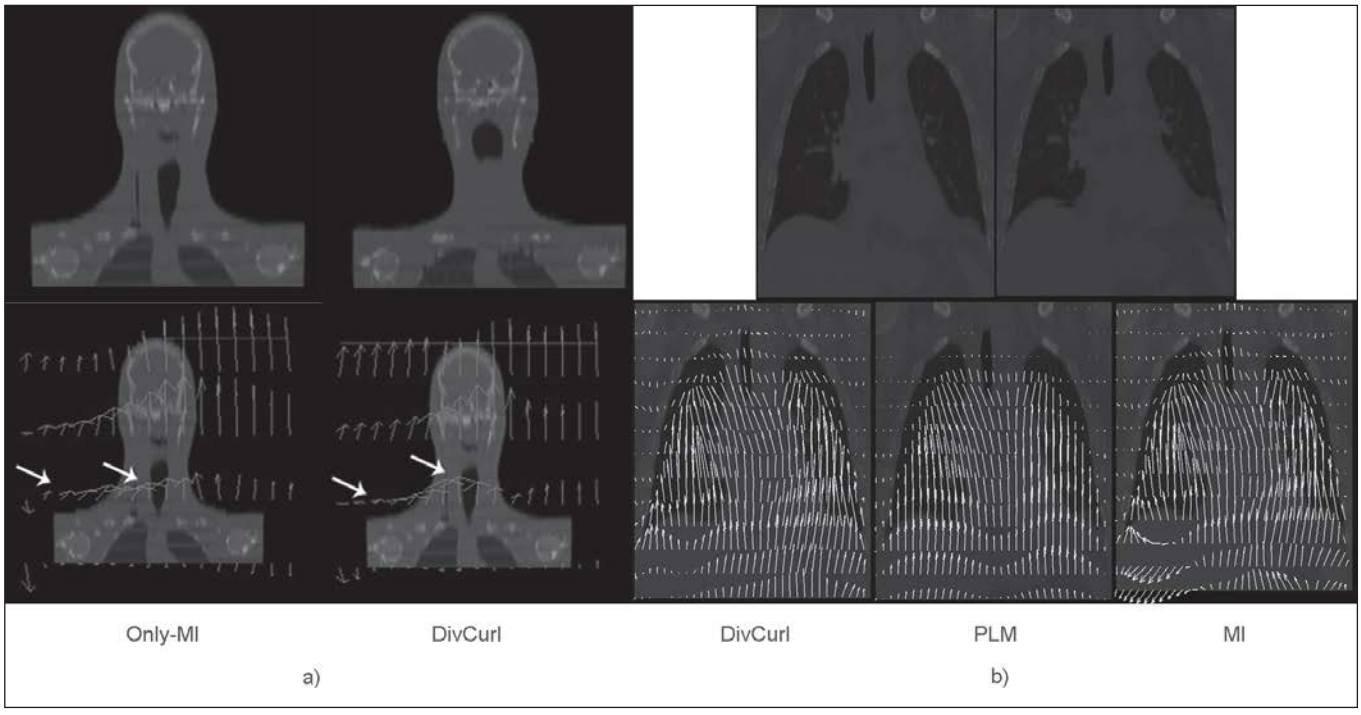

Figure 4 One slice of warped images belonging to the synthetic cases and ClinicCase1 are overlaid on final DF for each method. Panel (a): first row represents fixed and moving image from left to right respectively for synthetic case, while the bottom row shows warped images belonging to only-MI and DivCurl method from left to right. The critically discriminative parts are represented by bold white arrows, to show the different behavior. Panel (b): first row shows the fixed and moving images, while the bottom row presents DF overlaid on warped images belonging to DivCurl, PLM and MI-only registrations aligned from left to right.

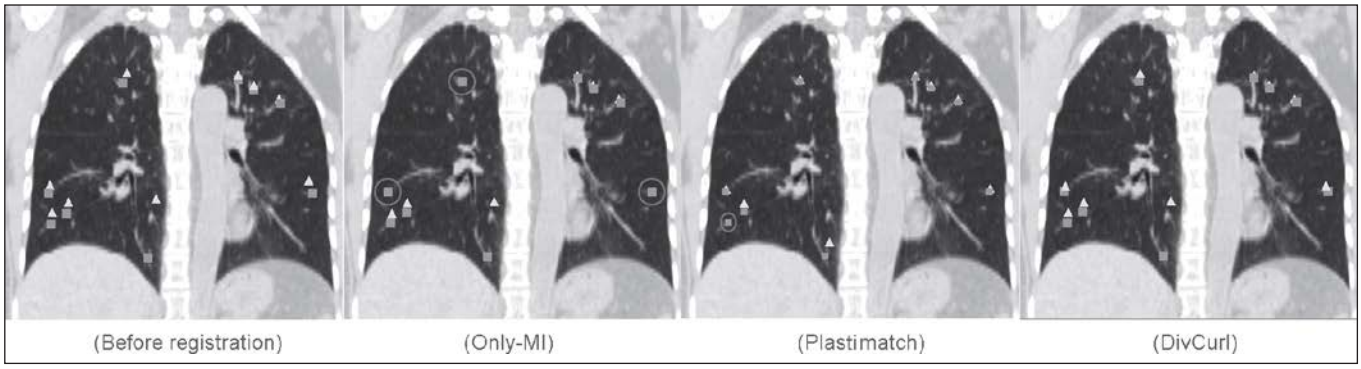

Figure 5 Landmark visualization in coronal view, where only landmarks in the current slice are shown for each method. Left image represents the alignment of reference landmarks (squares) and target landmarks (triangles) on fixed image of ClinicCase1 before the registration, while next middle-left image shows the warped landmarks for Only-MI method. In middle-right the reference landmarks (squares) and the warped landmarks (triangles) are overlaid after the registration for DivCurl method, whereas in the right image the landmark correspondence for PLM is illustrated. Circles are depicted around landmarks that are not registered due to inaccurate compensation.

Curl, PLM and Only-MI method respec -tively. Both PLM and DivCurl resulted in a smoother deformation field, as demon-strated by the distribution of the vector field in the liver region. The MI method ex-hibited physiologically inconsistent de-formation in the liver due to the lack of regularization in a homogeneous region.

Finally, registration running time considering the ClinicCase1, for MI-only method is about 420 sec, whereas PLM method requires 1400 sec and DivCurl takes 3100 sec, due to additional computation of div and curl regularization terms at each iteration.

3.3 Landmark Errors Evaluation

We measured the average 3D Euclidean distance between reference manual landmarks and warped landmarks after registration (Table 2). In Figure 5, 2D visualization of this approach is presented for the sake of qualitative evaluation. The left

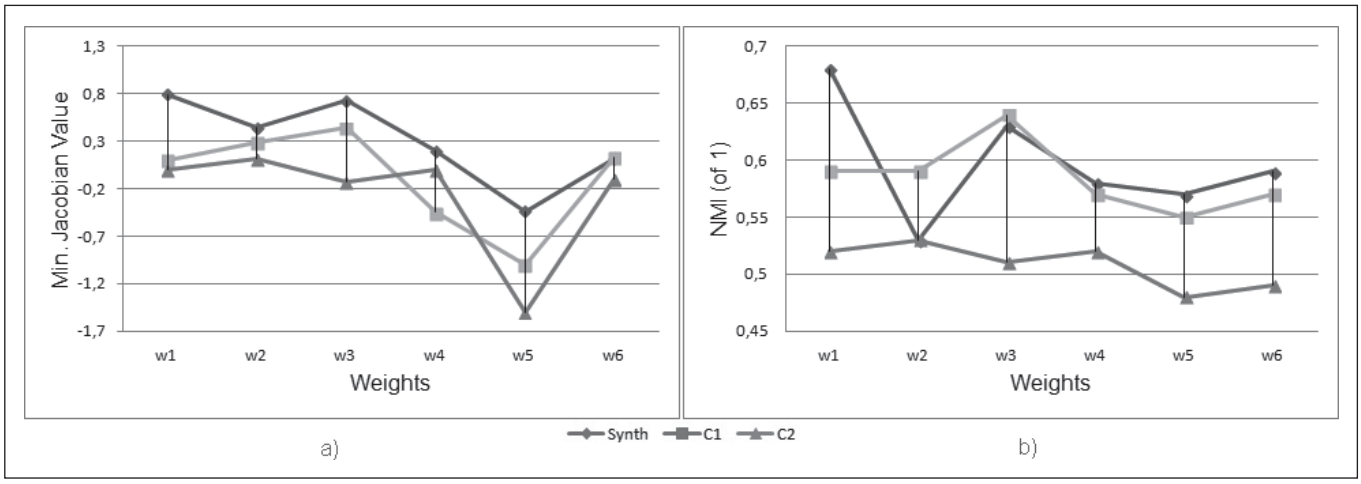

Figure 6 Weight assessment with respect to different test cases. (a) represents min. jacobian value evaluation for synthetic, ClinicCase1 and ClinicCase2, whereas (b) shows NMI values both with respect to combination of different specific weights. (w1 = [0.1, 0.1, 0,0], w2 = [1, 1, 0, 0], w3 = [0.5, 0.5, 0.5, 0.5], w4 = [0, 0, 1, 1], w5 = [4, 0, 4, 0], w6 = [0, 1, 0, 1]).

image illustrates the reference landmarks at inhale (squares) and target landmarks at exhale (triangles) on the fixed image of ClinicCase1 before the registration, followed by the same overlay resulting from the presented methods (Only-MI, DivCurl, PLM). In Figure 5, circles around some local points which are not registered due to misalignment during the optimization process comparing to before registration are shown. If we now concentrate on the regularized methods, it is possible to see how local discontinuities have been compensated in both regularized methods.

4. Discussion

We successfully implemented a multi-modal and multi-stage registration framework to obtain regularized deformable image registration of 3D medical images based on divergence/curl regularization (DivCurl). This was tested in synthetic and clinical cases to show the performance of the proposed method, to be compared with non regularized (Only-MI) registration and alternative regularization strategies (PLM).

4.1 Optimal Div-curl Weights

Different performance was achieved by varying the weights assigned to div/curl operators for each dataset. Specific studies are required to determine the optimal weights for specific registration problems, in terms of images anatomical site and expected deformation amplitude. A general behavior was highlighted in the dataset available for this work, which might serve as the starting point for future investigations. Figure 6a and Figure 6b show combination of different weights to evaluate the smoothness of DF as well as residual intensity difference for Synthetic, Clinic-

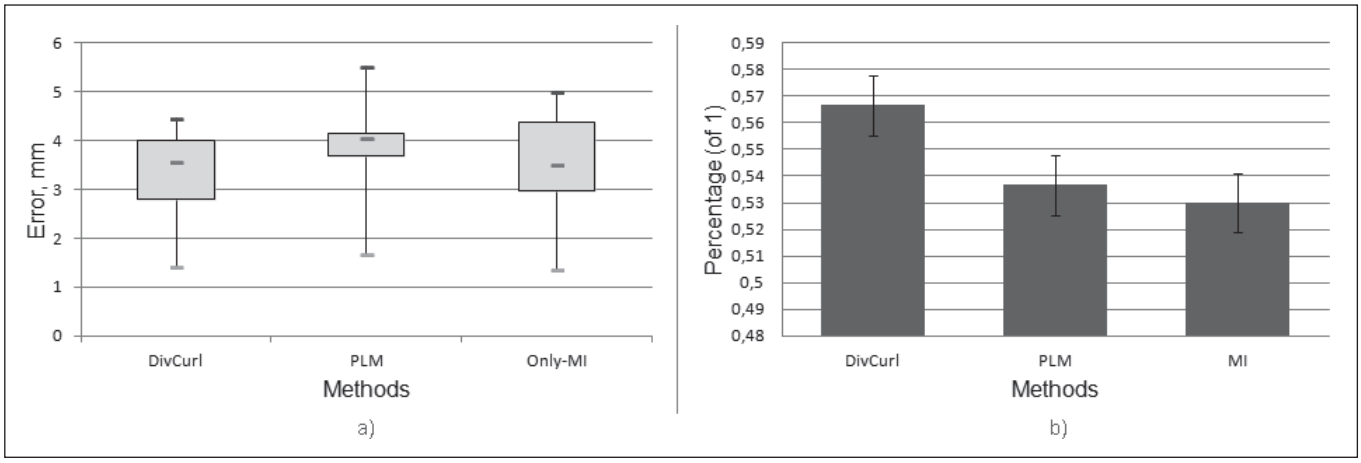

Figure 7 a) Box plot represents distribution of the landmark errors on all the clinical experiments for each method. b) Average NMI values for each method, demonstrating higher image similarity by DivCurl.

Case1 and ClinicCase2 by using min. Jacobian (a) and NMI (b). Combinations are presented in the caption of Figure 6. Based on Figure 6, it is possible to ob-serve that we obtained smoother final DF for the cases where the coefficients in coarser grid are larger than in the fine grid (w1, w2), especially in terms of minimum jacobian value. Conversely, the use of a single regularization function (either div or curl) led to sub-optimal results (w5, w6). The latter fact is proved on phantom cases, where the smoothest DF was obtained when the fine stage coefficients were set to zero. Figure 6 proves that w1 fits the best for synthetic case and w3 and w2 are the most optimal weights for clinic cases 1 and 2 respectively, in terms of both metrics. This weight combination might be used for any type of dataset, but the optimal configuration is intrinsically case dependent.

4.2 Comparison with Non- regularized Methods

As can be conceived by the cost function (Figure 2), the combination of probabil-ity density based MI metric and the direct voxel-intensity based div/curl regularization term is not trivial. Both in [12] and [13], the author use SSD of the intensities to adjust the similarity between the images, restricting the applicability of their method to mono-modal cases with equal gradient scales. Our method instead has the potential to address the problem of non-physical registration compensation also in multi-modal image applications.

As visible from Table 2, we obtained smoother final DF with less irregularity, along with an enhanced image similarity compared to non-regularized registration method. For the synthetic cases, we reported 8.5% of improvement in terms of RMS displacement field, compared to the MI-only method. In the clinical dataset, NMI values for the DivCurl method were consistently larger than Only-MI registration, thus proving that the use of regularization function is able to achieve better similarity than unconstrained (i.e. non regularized) methods. Similar considerations can be extended to the inverse consistency and landmark error evaluation. Improvements of DivCurl with respect to Only-MI in clinical cases were as high as 39% (ClinicCase3) for inverse consistency and 11% (ClinicCase2) for the landmark error evaluation.

4.3 Comparison with Plastimatch

We compared our results with a Bspline based Plastimatch method where the regularization term is used during the optimization at each iteration, in opposition to other algorithms where regularization is achieved through a smoothing term applied after optimization. In this perspective, the selected method is analogous to DivCurl implementation, which differs in terms of selected quantities for regularization. The box plot in Figure 7a summarizes the distribution of the landmark errors for each method, quantified on the clinical dataset. PLM resulted in significantly higher errors, as confirmed by the statistical analysis (3.8 mm for PLM, versus 3.3mm for DivCurl and 3.4mm for Only-MI). In Figure 7b, we report the distribution of NMI values for each method, showing that higher similarity was obtained by DivCurl compared to PLM. Statistical analysis (non parametric Friedman test) revealed that NMI values are statistically different at 99% confidence. The post-hoc comparison highlighted that DivCurl features significantly higher NMI values compared to the MI method, whereas no significant difference exist with the PLM algorithm. As for inverse consistency errors, it is clearly visible from Table II that the DivCurl method yielded consistently reduced errors in all clinical cases, if compared to PLM.

5. Conclusion

We achieved successful integration of divergence and curl regularization terms in a multi-resolution deformable image registration method using ITK libraries. The method was tested both on 3D CT cervical synthetically deformed phantom images and 4D CT pulmonary patient images.

After registration, we compared our method with another regularization strategy based on second derivatives, as well as with non-regularized method. As a result, statistical analysis performed on two evaluation metrics (i.e. Landmark Registration Error and NMI) revealed significantly higher values for our implementation with respect to both methods.

Future work will consist in the development of an automatic strategy for deriving optimal registration parameters for each patient case, as well as porting the method to GPUs, in order to reduce the computational cost.

References

1. Kaus MR, Brock KK. Deformable image registration for radiation therapy planning: Algorithms and applications. In: Leondes CT, editor. Biomechanical systems technology. World Scientific Publishing; 2007. pp 1–28.
2. Chao M, Xie Y, Xing L. Auto-propagation of contours for adaptive prostate radiation therapy. Phys Med Biol 2008: 53: 4533–4542.
3. Peroni M, Ciardo D, Spadea MF, Riboldi M, Comi S, Alterio D, et al. Automatic Segmentation and Online virtual CT in Head-and-Neck Adaptive Radiation Therapy. Int J Radiat Oncol Biol Phys 2012: 84 (3): 427–433.
4. Riboldi M, Orecchia R, Baroni G. Real-time tumour tracking in particle therapy: technological developments and future perspectives. Lancet Oncol 2012: 13: 383–391.
5. Torshabi AE, Pella A, Riboldi M, Baroni G. Targeting accuracy in real-time tumor tracking via external surrogates: a comparative study. Technol Cancer Res Treat 2010: 9: 551–562.
6. Seregni M, Pella A, Riboldi M, Orecchia R, Cerveri P, Baroni G. Real-time tumor tracking with an artificial neural networks-based method: A feasibility study. Phys Med Forthcoming 2011.
7. Schaerer J, Fassi A, Riboldi M, Cerveri P, Baroni G, Sarrut D. Multi-dimensional respiratory motion tracking from markerless optical surface imaging based on deformable mesh registration. Phys Med. Biol 2012: 57: 357–373.
8. Sarrut D. Deformable registration for image-guided radiation therapy. Z Med Phys 2006: 16: 285–297.
9. Rueckert D, Sonoda LI, Hayes C, Hill DLG, Leach MO, Hawkes DJ. Nonrigid registration using free-form deformations: Application to breast MR images. IEEE Transactions on Medical Imaging 1999: 18: 712–721.
10. Staring M. Regularization in deformable registration. 13th International Conference on Medical Image Computing and Computer Assisted Intervention; Beijing, China; 2010.
11. Vercauteren T, Pennec X, Perchant A, Ayache N. Non-parametric diffeomorphic image registration with the demons algorithm: Medical Image Computing and Computer-Assisted Intervention (MICCAI); 2007: Lecture Notes in Computer Science 2007: 4792: 319–326.
12. Sorzano CS, Thévenaz P, Unser M. Elastic registration of biological images using vector-spline regu-

larization. IEEE Transactions on Biomedical Engineering 2005: 52: 652 –563.
13. Arganda-Carreras I, Sorzano CS, Marabini R, Carazo JM, Ortiz-de Solorzano C, Kybic J. Consistent and elastic registration of histological sections using vector-spline regularization. Proceedings of the Second ECCV international conference on Computer Vision Approaches to Medical Image Analysis; 2006. Berlin, Heidelberg: Springer-Verlag 2006. pp 85 –95.
14. Klein S, Staring M, Pluim JP. Evaluation of optimization methods for nonrigid medical image registration using mutual information and B-splines. IEEE Transactions On Image Processing 2007: 16: 2879 –2890.
15. Ibanez L, Schroeder W, Ng L, Cates J. The ITK software guide. Insight Toolkit Kitware Inc: 2003.
16. Rohlfing T. Image Similarity and Tissue Overlaps as Surrogates for Image Registration Accuracy: Widely Used but Unreliable. IEEE Transactions on Medical Imaging 2012: 31 (2): 153–163.
17. Plastimatch [Internet]. Available from http://www.plastimatch.org.
18. Peroni M, Golland P, Sharp GC, Baroni G. Ranking of stopping criteria for log domain diffeomorphic demons application in clinical radiation therapy. 33rd Annual International Conference of the IEEE EMBS: Conf Proc IEEE Eng Med Biol Soc; 2011. pp 4884 – 4887.
19. Rohlfing T, Maurer CR, Bluemke Jr, DA, Jacobs MA. Volume-preserving nonrigid registration of MR breast images using free-form deformation with an incompressibility constraint. IEEE Transactions on Medical Imaging 2003: 22: 730–741.
20. Urschler M, Kluckner S, Bischof H. A Framework for comparison and evaluation of nonlinear intra-subject image registration algorithms. Institute of Computer Graphics and Vision, Graz, University of Technology, Austria. Insight Journal 2008.
21. Sharp GC, Li R, Wolfgang J, Chen G, Peroni M, Spadea MF, et al. Plastimatch – An open source software suite for radiotherapy image processing. Proceedings of the XVIth International Conference on the use of Computers in Radiotherapy (ICCR); Amsterdam, Netherlands.